Characterization of the biofilm landscape of *Bacillus subtilis* by spatial microproteomics

AUTHORS:

Kevin J. Zemaitis[1]*, Mowei Zhou[1,+], Sarah M. Yannarell[3,4], James M. Fulcher[1], Arunima Bhattacharjee[1], Marija Veličković[1], David J. Degnan[2], Elizabeth A. Shank[5], Christopher R. Anderton[1], William Kew[1], Ljiljana Paša-Tolić[1], Dušan Veličković[1]*

AFFILIATIONS:

[1]Environmental Molecular Sciences Laboratory, Pacific Northwest National Laboratory, Richland, Washington, USA

[2]Biological Sciences Division, Pacific Northwest National Laboratory, Richland, Washington, USA

[3]Department of Microbiology and Immunology, University of North Carolina at Chapel Hill, Chapel Hill, North Carolina, USA

[4]Department of Biology, University of North Carolina at Chapel Hill, Chapel Hill, NC, USA

[5]Department of Systems Biology, University of Massachusetts Chan Medical School, Worcester, Massachusetts, USA

[+]Present affiliation: Department of Chemistry, Zhejiang University, Hangzhou, Zhejiang 310058, China

CORRESPONDING AUTHOR(S):

*Kevin J. Zemaitis – Email: kevin.zemaitis@pnnl.gov

*Dusan Veličković – Email: dusan.velickovic@pnnl.gov

GRAPHICAL ABSTRACT

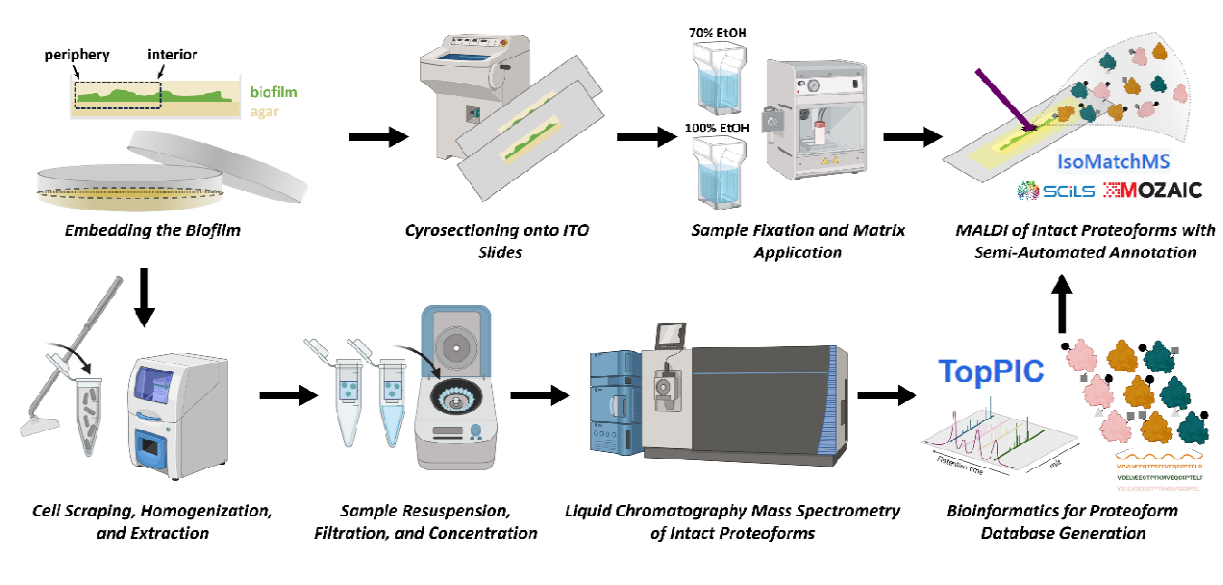

KEYWORDS: Bioanalytical methods, Mass spectrometry imaging, Proteoforms, Bacterial biofilms, MALDI

ABSTRACT

Bulk proteomics has been demonstrated to differentiate subpopulations based on molecular phenotypes within bacterial colonies, yet advanced analyses by mass spectrometry imaging (MSI) hold even greater promise for the future. This technology can enable high-throughput spatial phenotyping that can directly visualize distinct components of various biomolecular mechanisms with high mass resolving power in high spatial resolution analyses. Here, we applied MSI for intact protein imaging directly from thin cross sections of a biofilm of *Bacillus subtilis* and after minimal preparation we detected more than 285 unique isotopic envelopes corresponding to unique proteoforms. We paired our MSI analyses with bulk top-down proteomics (TDP) to form extensive experimental libraries which provided us with high confidence in MSI annotations based upon isotopic matching to validated post-translational modifications (PTMs) and truncations. This joint application of MSI and TDP allowed us to describe the microscale spatial proteomic landscape within the *B. subtilis* biofilm analyzed. Further demonstrating the feasibility of detecting a few differentiated subpopulations through identification of toxic cannibalistic proteoforms as well as those involved in active sporulation to highly localized areas within the central and outermost periphery of the biofilm.

INTRODUCTION:

Bacillus subtilis biofilms form distinct spatial microenvironments where unique biological functions such as sporulation, colonization, and metabolite production are governed by underlying mechanisms.(1, 2) The proteins within these biochemical mechanisms can be used as proxies to localize cellular phenotypes from the central core to the outer periphery of a colony.(3) Not only are these subpopulations spatiotemporally dynamic, but they directly result from differential genetic expression,(4) with mutations driving further heterogeneous responses.(5) Using *B. subtilis* as a model organism for biofilm development,(6) we conducted top-down proteomics (TDP) and matrix-assisted laser desorption/ionization (MALDI) mass spectrometry imaging (MSI) on thin sections of the biofilm to explore the intact protein landscape revealing differentiated subpopulations.(7, 8) While MSI has been broadly applied within microbiology for the detection of primary and secondary metabolites, and highly abundant lipids.(9) The detection of intact proteins distributions hold unique promise;(10) where species, subpopulations, and molecular phenotypes can be identified by differentially abundant proteins within unique biochemical mechanisms in a manner similar to spatial biotyping.(11)

Similar works have focused upon MALDI-MSI of small toxic peptides within *B. subtilis* (e.g., sporulation delay protein, SDP; sporulation killing factor, SKF; and epipeptide, EPE),(12) which traced cannibalistic cell-types in wild-type and knockout mutants. In addition to MALDI-MSI mapping the localization of these cannibalistic toxins,(12) further insight has been drawn into the function and interdependence of these toxic peptides in the control of sporulation and further biofilm development through genetic knockouts.(13) Demonstrating that in parallel application MALDI-MSI is an enabling tool for microbiology, where the direct localization of lipids, primary and secondary metabolites, and toxic peptides enhance more traditional spectroscopy completed on cultured biofilms. Here, we demonstrate discovery-based efforts for contextualization of spatial dependencies of intercellular and extracellular proteins,(14) providing the location of larger abundant proteomic mechanisms responsible for cellular differentiation and biofilm production.(10)

METHODOLOGY:

78 *Top-Down Sample Preparation of B. subtilis*

79 For TDP, *B. subtilis* was cultured similarly to as previously described before on MSgg agar
80 plates.(1) After 48 hours of growth isolated *B. subtilis* colonies were scraped with a cell scraper
81 and collected in Eppendorf tubes. These tubes were subsequently frozen
82 and lyophilized. The lyophilized sample was bead beaten with a 3 mm tungsten carbide bead at
83 1,400 c.p.m. for 2 min using a HG-600 Geno/Grinder 2010 Tissue Homogenizer and
84 Cell Lyser (Cole Palmer, Metuchen, NJ), using cooled cryoblocks to inhibit sample heating.
85 Briefly, powdered sample was resuspended in Type 1 water and cold (−20 °C)
86 chloroform:methanol mixture (2:1, *v/v*) in chloroform-compatible 2 mL Sorenson MulTI
87 SafeSeal microcentrifuge tubes (Sorenson Bioscience, Salt Lake City, UT). The sample was vortex
88 mixed for 1 min, followed by incubation on ice for 5 min, then vortexed again for 1 min and
89 centrifuged at 10,000 g at 4 °C for 10 min. The top and bottom phases were discarded. The
90 remaining protein interlayer was washed with cold 100% methanol, vortexed, and centrifuged
91 for 5 min to pellet the protein. Supernatant was discarded. The protein interlayer was
92 resuspended in 8 M urea prepared in 50 mM ammonium bicarbonate (pH 8). Samples were
93 subsequently cleaned and concentrated using Amicon ultra centrifugal filtration molecular
94 weight cutoff (MWCO) filter tubes (Millipore, Bedford, MA) following the manufacturers
95 standard operating procedure for centrifuging at 14,000 g. Filtration starting first with a 100
96 kDa filter resulting in concentrated protein which was subsequently transferred to a 10 kDa
97 MWCO filter for desalting. After filtration the protein concentration was determined using a
98 bicinchoninic acid (BCA) assay (Thermo Scientific, Waltham, MA) and samples were diluted to
99 0.5 µg/µL in water with 0.1% FA.

100 *Top-Down Liquid Chromatography Mass Spectrometry*

101 Liquid chromatography mass spectrometry (LC-MS) was completed on both an Exploris 480
102 Orbitrap MS (Thermo Scientific, Bremen, DE) and a Lumos Tribrid Orbitrap MS (Thermo
103 Scientific, San Jose, CA) injecting protein onto a NanoAcquity (Waters, Millford, MA) with dual
104 pumps configuration, use of multiple instruments was for validation and is not required for
105 successful TDP. Binary solvents for mobile phase (MP) A and B were 0.2% formic acid in water

106 (MPA), and 0.2% formic acid in acetonitrile (MPB) for both pumps. The stationary phase
107 material for in-house packed reversed phase LC columns was C2 particle (SMTC2MEB2-3-300,
108 Separation Methods Technologies, Newark, DE). 10 µl injections were loaded onto a short trap
109 column (150 µm i.d., 5 cm long) and desalted with a flow of 3 µl/min with 5% MPB for 5 min.
110 Then the trap column was switched to the analytical column (100 µm i.d., 50 cm long) with flow
111 rate of 0.3 µl/min. Separation gradient started at 5% MPB to 15% MPB over 1 minute and was
112 linearly ramped to 90% MPB over 89 min.

113 The Exploris 480 Orbitrap MS (Thermo Scientific, Bremen, DE) was operated with the following
114 source parameters including a spray voltage of 2.2 kV, transfer capillary temperature of 275 ˚C,
115 and ion funnel RF amplitude set to 60%. The instrument was set to "intact protein" application
116 mode with standard pressures, and data was collected as full profile. MS1 acquisitions were
117 collected with 5 microscans at a mass resolution setting of 120k over a scan range of *m/z* 500 to
118 2000 with a normalized AGC target of 400%. Data dependent MS2 scans were collected with 2
119 microscans over a scan range of *m/z* 300 to 2000 with a normalized AGC target of 1000%. MS2
120 used a dynamic exclusion after 1 time over a duration of 40s with an isolation window of ±2
121 *m/z* with fragmentation by HCD at a fixed normalized collision energy of 35%.

122 The Lumos Tribrid Orbitrap MS (Thermo Scientific, San Jose, CA) was operated with the
123 following source parameters including a spray voltage of 2.2 kV, transfer capillary temperature
124 of 275 ˚C, and ion funnel RF amplitude set to 50%. The instrument was set to "peptide"
125 application mode with standard pressures, and data was collected as full profile. MS1
126 acquisitions were collected with 3 microscans at a mass resolution setting of 120k over a scan
127 range of *m/z* 400 to 2000 with a normalized AGC target of 200%. Data dependent MS2 scans
128 were collected with 1 microscans over a scan range of *m/z* 300 to 2000 with a normalized AGC
129 target of 500% and maximum injection time of 118 ms. MS2 used a dynamic exclusion after 1
130 time over a duration of 60s with an isolation window of ±1 *m/z* with fragmentation by HCD at a
131 stepped collision energy of 20V, 30V, and 40V.

132 *Top-down proteomics data analysis*

133 MS instrument ".RAW" files were first converted into ".mzML" format with MSConvert before
134 processing with the open-search software TopPIC Suite (version 1.4.13).(15) For TopFD
135 deconvolution, a precursor window of 1 and 2 *m/z* corresponding to the Lumos and Exploris
136 respectively, error tolerance of 0.02 *m/z*, MS1 signal to noise ratio (SNR) of 3, MS2 SNR of 1,
137 maximum charge of 30, and maximum monoisotopic mass of 50,000 Da were applied. Specific
138 settings for the TopPIC search included an error tolerance of 15 ppm, PrSM cluster tolerance of
139 3.2 Da, FDR of 0.01, and a maximum and minimum unknown mass shift of ±500 Da, and a
140 maximum of one unknown mass shift.

141 *Thin Bacterial Biofilms Production for Imaging*

142 For MALDI-MSI *B. subtilis* were cultured on MSgg growth medium as previously described,(2)
143 and a thin sectioning protocol was applied as described in greater depth elsewhere.(16, 17)
144 Briefly, the biofilm agar blocks were quartered and transferred to molds (22-363-553, Fisher
145 Scientific). These molds were then snap frozen at -80 °C, overlaid with 4% (wt/vol) agarose
146 (Lonza Bioscience) and frozen at -80 °C for 15 min. Sectioning was completed as previously
147 reported using a Cryostar NX70 cryotome (Thermo Scientific, Runcorn, UK) and cross-sections
148 were taken at 20 µm thickness onto ITO slides (Bruker Daltonics, Bremen, DE). These sections
149 were stored at -80 °C until analysis.

150 *Preparation for Intact Proteoform Imaging*

151 Slides were prepared for MALDI by vacuum desiccating at -15 inHg for 30 min with subsequent
152 washing in a two-part series for prior to matrix deposition. Washing was completed with
153 submersion in a solution of 70% ethanol for 30 sec, then submersion in a solution of 100%
154 ethanol for 30 sec. After which, the biofilms were then dried by a gentle stream of nitrogen for
155 30 sec. A M5 Sprayer (HTX Technologies, Chapel Hill, NC) was then used to spray the surface
156 with 5 crisscross (CC) passes of a solution of 5% acetic acid (v/v) in 50% ethanol with a flow rate
157 of 150 µL/min, a nozzle temperature of 30.0 °C, and the velocity set to 1,250 mm/min with 10
158 PSI of nitrogen gas to boost proteoform signal intensity.(18) A 5 s drying period was added
159 between each of the passes with a 3 mm track spacing, the same sprayer was then immediately
160 used to deposit 15 mg/mL 2,5-DHA in 90% acetonitrile with 0.2% TFA. Only the supernatant of

161 the dissolved matrix was sprayed after sonication and centrifugation. The flow rate of the
162 matrix was 150 µL/min with a nozzle temperature of 30.0 °C, and the velocity was set to 1,300
163 mm/min with 10 PSI of nitrogen gas. The matrix was applied with a 2 mm track spacing and a
164 crisscross pattern, and the matrix coverage was calculated to be 277 µg/cm^2. The matrix was
165 then recrystallized with 5% acetic acid solution (v/v) in water at 38.5 °C and dried for 3.5 min,
166 using an apparatus similar to that previously reported.(19)

167 *MALDI Mass Spectrometry Imaging of Sectioned Biofilms*

168 An elevated pressure (EP) MALDI source with an atmospheric pressure ionization inlet
169 (Spectroglyph, LLC, Kennewick, WA) was mounted on a research grade Q Exactive HF Orbitrap
170 MS (Thermo Scientific, Bremen, DE), this instrument was upgraded with ultrahigh mass range
171 (UHMR) boards and operated under custom privileges licenses. This platform is described in
172 greater depth elsewhere,(20) briefly, the MALDI source was operated at 7.8 Torr, with fore
173 vacuum of the spectrometer at 1.0 mbar, and an ultrahigh vacuum adjusted to 2.54e-10 mbar
174 with argon gas. Spectra were acquired over a *m/z* range of 2,000 to 20,000, and acquisitions
175 were carried out with preset resolution of 240k, resulting in a transient of 512 ms, and
176 observed mass resolving power of 45k at *m/z* 6,725. The laser diode of the Explorer One 349
177 nm Nd:YLF (Spectra-Physics, Milpitas, California) was set to output an average of 1.1 µJ/pulse at
178 1 kHz, and ion were accumulated for 500 ms – resulting in 500 laser shots per pixel. Imaging
179 was carried out at 20 µm spatial resolution, and the resultant desorption of the crater
180 measured by light microscopy was found to be roughly 12 µm × 15 µm, which did not
181 oversample the surface.

182 *Mass Spectrometry Imaging Data Analysis*

183 Visualization was completed with automatic import of the .RAW acquisition file and .xml of the
184 pixel coordinates into SCiLS Lab Pro (v.2021c, Bruker Daltonics, Bremen, DE). Ion images were
185 generated by extracting singular isotopic peaks for the proteoforms after root mean square
186 normalization (RMS). For proteoform assignments, an experimental library of proteoforms from
187 TDP LC-MS/MS were used as custom databases and isotopic profiles were manually matched
188 and mass shifts annotated. Mozaic (v.2023.4.0.b3, Spectroswiss, Lausanne, CH) was used to

189 average the 34,698 acquisitions within the MALDI-MSI experiment, after averaging the spectra
190 was baseline corrected using the model-free method with a median size of 250, and other
191 default parameters for number of points, sigma, iterations and level (11, 5, 1, 1). A developed
192 package IsoMatchMS, was used to generate candidate matches based on isotopic distribution
193 matching, this package is explained in greater depth elsewhere.(21) Briefly, an entire average of
194 the acquisition file was exported as a .mzML file after processing. This file was imported with
195 annotations and accurate masses with <5 ppm error were considered, and further filtering of
196 the matches occurred with Pearson correlation score of ≥0.7. Further manual verification of
197 annotated and non-annotated proteoforms were searched against multiple adducts.

198 **RESULTS AND DISCUSSION:**

199 Through spatial proteomics we provide direct insights into differentiated
200 subpopulations. Previous analyses of these samples had identified distinct distributions of lipids
201 and surfactants,(2) and here an optimized sample preparation which included mild ethanol
202 fixation enabled the detection of intact protein distributions **(Figure 1a)**, and further desalting
203 was found to not be necessary unlike within mammalian and plant tissues previously analyzed
204 on this platform, or within colonies dried directly onto ITO slides and analyzed from the top
205 down (22). Analyses of these samples were enabled by coupling a MALDI source to a research
206 grade UHMR HF Orbitrap MS,(18) this combination yields rich spectra with high intensities of
207 intact proteins and proteoforms, up to 20 kDa in mass **(Figure 1r)**, although the highest
208 detected species from the biofilm was roughly 13.5 kDa.(23) Subsequently, we performed semi-
209 automated annotation and evaluation of the proteomic spatial heterogeneity within the
210 biofilm. Overall, more than 285 unique isotopic envelopes from proteoforms were detected
211 **(Figure 1r)** and can be annotated via UniProt or experimentally generated TDP libraries –
212 enabling precise annotation of PTMs and truncations.(24) Manual validation was performed
213 after isotopic matching,(21) and sample-specific TDP libraries were imperative for the
214 successful annotation of ion images.

215 Of the proteoform distributions, characteristic toxic peptides (e.g., SDP) are seen within
216 the active interior of the biofilm **(Figure 1c)**,(25) while sporulating proteins **(Figure 1i, 1k, 1m)**
217 and further uncharacterized proteins **(Figure 1o, 1q)** were found within the outer periphery.

218 The presence of SDP **(Figure 1c)** in the central core of the colony can be indicative of
219 cannibalistic cells recycling older generations, but the absence within the outer periphery and
220 presence of characteristic sporulating proteins highly localized to the outermost periphery
221 **(Figure 1i, 1k, 1m)**, suggests the biofilm is in early phases of sporulation. Stage V sporulation
222 protein S can be overcome by other proteins or mutation,(26) but through colocalization of
223 small acid-soluble spore (SASP) protein J **(Figure 1k)**, the presence of sporulated cells can be
224 confirmed where SASPs are roughly 20% of the outer spore coat of *B. subtilis.*(27) These
225 findings are supported by recent reports of cannibalistic toxins tend to prolong and delay
226 sporulation,(13) further demonstrating the utility of the detection of intact proteoforms for
227 spatial subtyping of populations.

228 TDP also detected sporulating delaying protein (SdpC) and immunity protein (SdpI)
229 **(Supplementary Material)**, which offers immunity to cells through the sequestration of
230 SDP.(28) Demonstrating that tandem TDP of microbial colonies can complement MALDI-MSI
231 analyses with coverage of larger proteoforms. When paired with laser capture microdissection
232 (LCM), spatial/sub-sample specific proteoform information can be integrated readily.(29)
233 Additionally, if paired with fluorescence microscopy a robust multimodal pipeline to validate
234 subpopulations and phenotypes is created. Several ribosomal proteins, including large subunits
235 **(Figure 1b, 1f, 1l, 1n)** were also routinely annotated with initiator methionine truncations, and
236 small subunits **(Figure 1h, 1j)** were also located throughout the main body of the biofilm. The
237 broad detection of these ribosomal proteins lends credence to spatial biotyper analyses,(11)
238 where speciation and localization of microbial cultures is feasible based on proteomic
239 signatures. If these cocultured colonies of bacteria and fungi are analyzed, or when working
240 upon mutant knockouts or bioengineered strains, this information can be vital to understanding
241 intermicrobial colonization and organization while further informing upon the cellular
242 processes and phenotypes.

243 We identified many isotopic signatures which are resolved but separated by only a few
244 hundred mDa **(Figure 1s)**. This complexity highlights the importance of sample-specific
245 proteoform libraries and high mass-resolving power limiting this workflow to Fourier transform
246 (FT)-MS instruments. While current applications were limited by incompatibility of ITO glass

247 slides and LCM-TDP workflows,(29, 30) future works should leverage spatial LCM-TDP with
248 MALDI-MSI for proteoform-informed spatial proteomics.(24) For example, several annotations
249 would benefit from such serial analyses, such as the 7.1 kDa protein **(Figure 1q)** annotated as
250 either uncharacterized protein YhjA (O07555) with a putative disulfide, or regulatory protein
251 DegR (P68731) with higher mass error. While protein YhjA possesses a signal peptide (AA 1-27)
252 which is cleaved, and a high confidence disulfide link (C37↔C87) which was annotated due to
253 the mass shift, and is supported by AlphaFold structural predictions **(Supplementary Figure 1)**
254 even though it is not listed within UniProt.(31, 32) Functionally, DegR stabilizes DegU
255 phosphorylation with links to increased protease activity,(33) and regulates transition of motile
256 cells to sessile forms.(10) While mass spectral error is higher than current thresholds, this
257 demonstrates the limits of high-resolution accurate mass isotopic pattern matching. In either
258 case, these links major mechanisms producing miner cells which degrade extracellular
259 biopolymers and peptides(34) and potential interactions with cannibalistic toxins noted to
260 prolong sporulation.(13) It should be noted DegR was not detected by TDP, possibly due to
261 analysis of a different culture or growth period, while other proteins such as DegV (35) were
262 identified **(Supplementary Material)**. Overall, these results demonstrate that advanced
263 measurement science is primed for future microbial applications and further use of this
264 instrumentation and pipeline can potentially unravel functions of many uncharacterized or
265 understudied proteins with proper experimental design.

266 **CONCLUSIONS:**

267 This study demonstrates that proteoform-informed spatial proteomics can resolve the
268 biochemical heterogeneity that governs microbial differentiation within *B. subtilis* biofilms. By
269 integrating MALDI-MSI with sample specific TDP libraries, we detected more than 285
270 proteoforms and revealed several distinct spatial distributions corresponding to cannibalistic,
271 sporulating, and metabolically active subpopulations. These results show that
272 proteoform-informed MSI can directly map functional microenvironments, offering
273 mechanistic insight into the temporal progression of biofilm development. While these
274 experiments were completed within a model system of *B. subtilis*, these methods for MALDI-
275 MSI and TDP are universal and can be broadly applied to any microbial system that can be

276 cultured on solid media. Additionally, while this is functionally limited to small proteoforms (<
277 20 kDa) for MALDI-MSI, the information gathered at fine spatial resolutions significantly
278 enhances our understanding of the metabolic gradients and biomolecular mechanisms that
279 shape community structure. The ability to localize toxic peptides, sporulation-associated
280 proteins, ribosomal subunits, and uncharacterized proteins underscores the power of this
281 approach to uncover both known and previously unappreciated contributors to microbial
282 physiology.

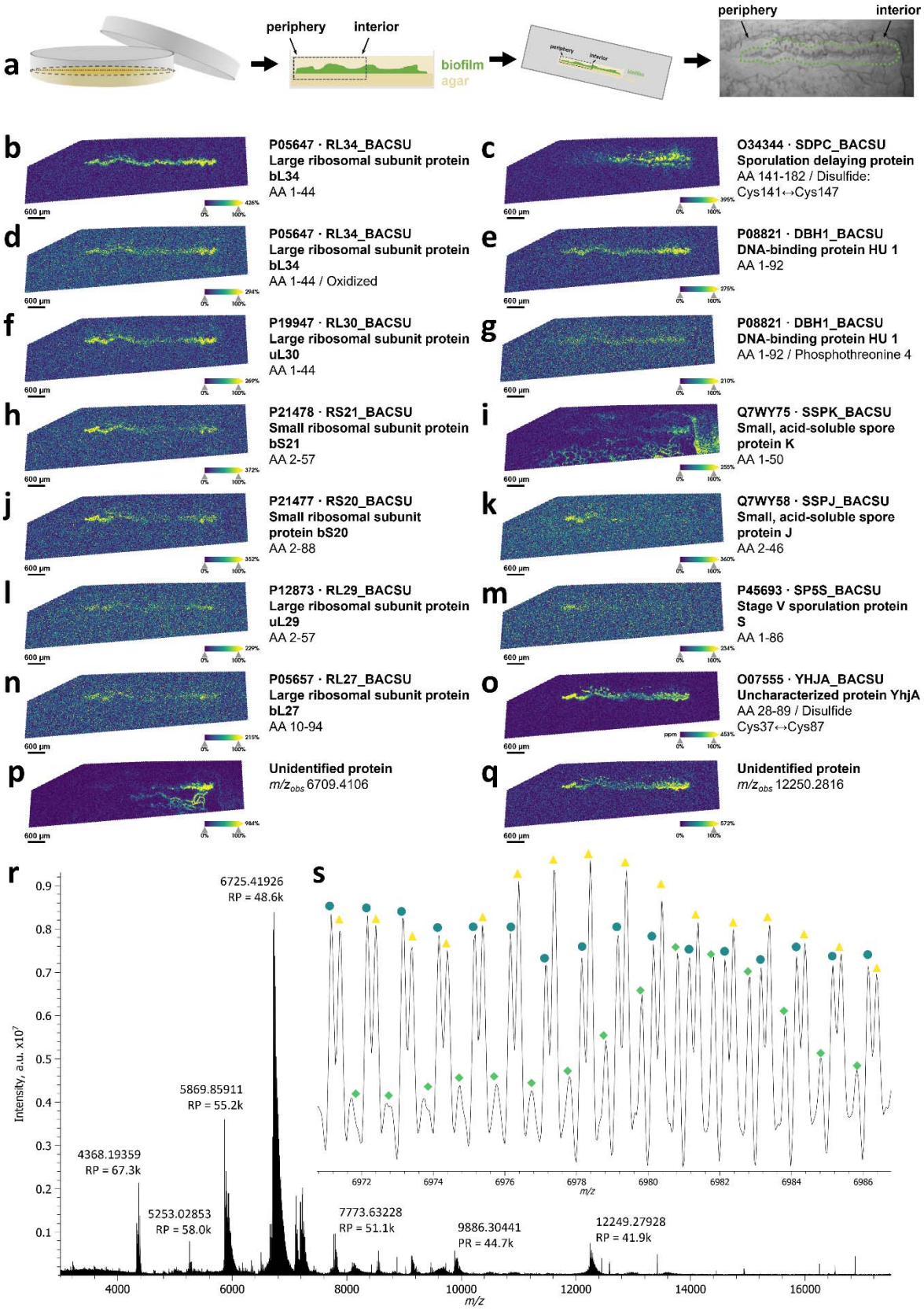
a
periphery
interior
biofilm
agar
periphery
interior
b
P05647 · RL34_BACSU
Large ribosomal subunit protein bL34
AA 1-44
c
O34344 · SDPC_BACSU
Sporulation delaying protein
AA 141-182 / Disulfide: Cys141↔Cys147
d
P05647 · RL34_BACSU
Large ribosomal subunit protein bL34
AA 1-44 / Oxidized
e
P08821 · DBH1_BACSU
DNA-binding protein HU 1
AA 1-92
f
P19947 · RL30_BACSU
Large ribosomal subunit protein uL30
AA 1-44
g
P08821 · DBH1_BACSU
DNA-binding protein HU 1
AA 1-92 / Phosphothreonine 4
h
P21478 · RS21_BACSU
Small ribosomal subunit protein bS21
AA 2-57
i
Q7WY75 · SSPK_BACSU
Small, acid-soluble spore protein K
AA 1-50
j
P21477 · RS20_BACSU
Small ribosomal subunit protein bS20
AA 2-88
k
Q7WY58 · SSPJ_BACSU
Small, acid-soluble spore protein J
AA 2-46
l
P12873 · RL29_BACSU
Large ribosomal subunit protein uL29
AA 2-57
m
P45693 · SP5S_BACSU
Stage V sporulation protein S
AA 1-86
n
P05657 · RL27_BACSU
Large ribosomal subunit protein bL27
AA 10-94
o
O07555 · YHJA_BACSU
Uncharacterized protein YhjA
AA 28-89 / Disulfide Cys37↔Cys87
p
Unidentified protein
m/z obs 6709.4106
q
Unidentified protein
m/z obs 12250.2816
600 µm
r
s
Intensity, a.u. x10^7
m/z
6725.41926
RP = 48.6k
5869.85911
RP = 55.2k
4368.19359
RP = 67.3k
5253.02853
RP = 58.0k
7773.63228
RP = 51.1k
9886.30441
PR = 44.7k
12249.27928
RP = 41.9k

283

284 **Figure 1.** The sample preparation is outlined within **(a)** showing colonies grown on MSgg media
285 which were further embedded and cryosectioned at 20 µm as outlined in **Supplementary**
286 **Information** and described in depth elsewhere.(2) After sample preparation, ion images are
287 shown for each proteoform, the name, UniProt accession ID, and amino acid sequence with
288 modifications (if any) are reported. Theoretical and experimental *m/z* values of the highest
289 abundance isotope with calculated error can be found within **Supplementary Information**. **(b)**
290 Large ribosomal subunit protein bL34 (P05647), **(c)** sporulation delaying protein (SDP; O34344),
291 **(d)** oxidized large ribosomal subunit protein bL34 (P05647), **(e)** DNA-binding protein HU 1
292 (P08821), **(f)** large ribosomal subunit protein uL30 (P19947;), **(g)** phosphorylated DNA-binding
293 protein HU 1 (P08821), **(h)** small ribosomal subunit protein bS21 (P21478;), **(i)** small acid-
294 soluble spore protein K (Q7WY75), **(j)** small ribosomal subunit protein bS20 (P21477), **(k)** small
295 acid-soluble spore protein J (Q7WY58), **(l)** large ribosomal subunit protein uL29 (P12873), **(m)**
296 stage V sporulation protein S (P45693), **(n)** large ribosomal subunit protein bL27 (P05657), **(o)** a
297 7.1kDa protein, which is either uncharacterized protein YhjA (O07555) with a disulfide at
298 Cys37↔Cys87 resulting in a [-2.01565 Da] shift, or regulatory protein DegR (P68731) with
299 larger error, **(p)** a 6.1kDa unannotated protein, and **(q)** a 12.4kDa unannotated protein. The
300 average spectrum from MALDI-MSI **(r)** is shown from *m/z* 3000 to 17500, with the complexity
301 shown within an inset zoom **(s)** of the spectrum from *m/z* 6971 to 6987. Three distinct isotopic
302 signatures are contained within this region, resulting from complex ion adduct and PTMs.
303 **SMART** annotation:(36) **S** (step size, spot size, total pixels) = 20 µm, 12 µm x 15 µm, 33084
304 pixels; **M** (molecular confidence) = MS1, <5 ppm; **A** (annotations) = MS1 matching from TDP LC-
305 MS/MS; **R** (resolving power) = 48.6k at *m/z* 6725.4; **T** (time of acquisition) = 286 min.

306

307 **DECLARATIONS:**

308 *Conflicts of Interest/Competing Interests*

309 The authors declare no conflicts of interest or competing interests.

310 *Author contribution statement*

*Data availability statement:*The data presented within this article is publicly available and was uploaded to MassIVE, partner repository with the MassIVE accession: MSV000100434.

For now, manuscript reviewers can access the data via FTP using:

Server: massive-ftp.ucsd.edu

User: MSV000100434

Password: Spatial7303

*Funding*This work was performed at the Environmental Molecular Science Laboratory (EMSL), a Department of Energy (DOE) Office of Science User Facility sponsored by the Office of Biological and Environmental Research. This expanded research on samples from EUP 51105 (doi.org/10.46936/expl.proj.2019.51105/60000139, E.A.S.) was funded by the intramural program on project awards doi.org/10.46936/intm.proj.2019.51159/60000152 (W.K) at EMSL (grid.436923.9) operated under Contract No. DE-AC05-76RL01830.

Acknowledgements

The authors would also like to acknowledge Dr. Mikhail Belov at Spectroglyph, LLC as well as Dr. Gordon Anderson and Chris Anderson at GAA Custom Electronics, LLC for technical support for the MALDI source. We would also like to acknowledge Drs. Tobias Wörner, Kyle Fort, Maria Reinhardt-Szyba, and Alexander Makarov of Thermo Fisher Scientific for technical guidance and licensing of the instrument. We thank Dr. Matthew E. Monroe of Pacific Northwest National Laboratory for his assistance in depositing the raw proteomic data onto MassIVE.

SUPPLEMENTARY INFORMATION (50 words):

The following is provided as supplementary information for this article includes: (1) "Supplementary Information" outlining sample preparation, mass spectrometry methods, and data analysis, supplementary figure S1, and a supplementary table of highlighted annotations, and (2) "Supplementary Material" in an output table of the TDP results from both mass spectrometry instruments used.

REFERENCES:

1. Yannarell SM, Beaudoin ES, Talley HS, Schoenborn AA, Orr G, Anderton CR, et al. Extensive cellular multi-tasking within *Bacillus subtilis* biofilms. mSystems. 2023;8(4):e00891-22.
2. Yannarell SM, Veličković D, Anderton CR, Shank EA. Direct Visualization of Chemical Cues and Cellular Phenotypes throughout Bacillus subtilis Biofilms. mSystems. 2021;6(6):e0103821.
3. van Dijl J, Hecker M. Bacillus subtilis: from soil bacterium to super-secreting cell factory. Microbial Cell Factories. 2013;12(1):3.
4. Dergham Y, Le Coq D, Nicolas P, Bidnenko E, Dérozier S, Deforet M, et al. Direct comparison of spatial transcriptional heterogeneity across diverse Bacillus subtilis biofilm communities. Nature Communications. 2023;14(1):7546.
5. Branda SS, González-Pastor JE, Ben-Yehuda S, Losick R, Kolter R. Fruiting body formation by Bacillus subtilis. Proceedings of the National Academy of Sciences. 2001;98(20):11621-6.
6. Vlamakis H, Chai Y, Beauregard P, Losick R, Kolter R. Sticking together: building a biofilm the Bacillus subtilis way. Nature Reviews Microbiology. 2013;11(3):157-68.
7. Bisht K, Wakeman CA. Discovery and Therapeutic Targeting of Differentiated Biofilm Subpopulations. Frontiers in Microbiology. 2019;10.
8. Ravikumar V, Nalpas NC, Anselm V, Krug K, Lenuzzi M, Šestak MS, et al. In-depth analysis of Bacillus subtilis proteome identifies new ORFs and traces the evolutionary history of modified proteins. Sci Rep. 2018;8(1):17246.
9. Dunham SJB, Ellis JF, Li B, Sweedler JV. Mass Spectrometry Imaging of Complex Microbial Communities. Acc Chem Res. 2017;50(1):96-104.
10. Mielich-Süss B, Lopez D. Molecular mechanisms involved in Bacillus subtilis biofilm formation. Environ Microbiol. 2015;17(3):555-65.
11. Gekenidis M-T, Studer P, Wüthrich S, Brunisholz R, Drissner D. Beyond the Matrix-Assisted Laser Desorption Ionization (MALDI) Biotyping Workflow: in Search of Microorganism-Specific Tryptic Peptides Enabling Discrimination of Subspecies. Applied and Environmental Microbiology. 2014;80(14):4234-41.
12. Si T, Li B, Zhang K, Xu Y, Zhao H, Sweedler JV. Characterization of Bacillus subtilis Colony Biofilms via Mass Spectrometry and Fluorescence Imaging. J Proteome Res. 2016;15(6):1955-62.
13. Friebel L, Knepper J-P, Becker NS, Abbaszade G, Stückrath K, Soltwisch J, et al. Cannibalism Shapes Biofilm Structure and Composition in Bacillus subtilis. bioRxiv. 2025:2025.03.21.644447.
14. Karygianni L, Ren Z, Koo H, Thurnheer T. Biofilm Matrixome: Extracellular Components in Structured Microbial Communities. Trends Microbiol. 2020;28(8):668-81.
15. Kou Q, Xun L, Liu X. TopPIC: a software tool for top-down mass spectrometry-based proteoform identification and characterization. Bioinformatics. 2016;32(22):3495-7.
16. Marlow VL, Cianfanelli FR, Porter M, Cairns LS, Dale JK, Stanley-Wall NR. The prevalence and origin of exoprotease-producing cells in the Bacillus subtilis biofilm. Microbiology. 2014;160(Pt 1):56.
17. Vlamakis H, Aguilar C, Losick R, Kolter R. Control of cell fate by the formation of an architecturally complex bacterial community. Genes & development. 2008;22(7):945-53.
18. Zemaitis KJ, Veličković D, Kew W, Fort KL, Reinhardt-Szyba M, Pamreddy A, et al. Enhanced Spatial Mapping of Histone Proteoforms in Human Kidney Through MALDI-MSI by High-Field UHMR-Orbitrap Detection. Analytical Chemistry. 2022;94(37):12604-13.
19. Yang J, Caprioli RM. Matrix Sublimation/Recrystallization for Imaging Proteins by Mass Spectrometry at High Spatial Resolution. Analytical Chemistry. 2011;83(14):5728-34.
20. Zemaitis KJ, Veličković D, Kew W, Fort KL, Reinhardt-Szyba M, Pamreddy A, et al. Enhanced Spatial Mapping of Histone Proteoforms in Human Kidney Through MALDI-MSI by High-Field UHMR-Orbitrap Detection. Analytical Chemistry. 2022.

21. Degnan DJ, Zemaitis KJ, Lewis LA, McCue LA, Bramer LM, Fulcher JM, et al. IsoMatchMS: Open-Source Software for Automated Annotation and Visualization of High Resolution MALDI-MS Spectra. Journal of the American Society for Mass Spectrometry. 2023.
22. Veličković D, Zemaitis KJ, Bhattacharjee A, Anderton CR. Mass spectrometry imaging of natural carbonyl products directly from agar-based microbial interactions using 4-APEBA derivatization. mSystems. 2024;9(1):e00803-23.
23. Smith LM, Kelleher NL, Linial M, Goodlett D, Langridge-Smith P, Ah Goo Y, et al. Proteoform: a single term describing protein complexity. Nature Methods. 2013;10(3):186-7.
24. Zemaitis KJ, Fulcher JM, Kumar R, Degnan DJ, Lewis LA, Liao Y-C, et al. Spatial top-down proteomics for the functional characterization of human kidney. Clinical Proteomics. 2025;22(1):9.
25. Lamsa A, Liu W-T, Dorrestein PC, Pogliano K. The Bacillus subtilis cannibalism toxin SDP collapses the proton motive force and induces autolysis. Molecular microbiology. 2012;84(3):486-500.
26. Resnekov O, Driks A, Losick R. Identification and characterization of sporulation gene spoVS from Bacillus subtilis. Journal of Bacteriology. 1995;177(19):5628-35.
27. Moeller R, Setlow P, Reitz G, Nicholson Wayne L. Roles of Small, Acid-Soluble Spore Proteins and Core Water Content in Survival of Bacillus subtilis Spores Exposed to Environmental Solar UV Radiation. Applied and Environmental Microbiology. 2009;75(16):5202-8.
28. Ellermeier CD, Hobbs EC, Gonzalez-Pastor JE, Losick R. A Three-Protein Signaling Pathway Governing Immunity to a Bacterial Cannibalism Toxin. Cell. 2006;124(3):549-59.
29. Liao Y-C, Fulcher JM, Degnan DJ, Williams SM, Bramer LM, Veličković D, et al. Spatially Resolved Top-Down Proteomics of Tissue Sections Based on a Microfluidic Nanodroplet Sample Preparation Platform. Molecular & Cellular Proteomics. 2023;22(2).
30. Veličković M, Day LZ, Zemaitis KJ, Attah IK, Burnum-Johnson KE, Anderton CR, et al. Enhanced Spatial Proteomics and Metabolomics from a Single Tissue Section Using MALDI-MSI and LCM-microPOTS Platforms. Analytical Chemistry. 2025;97(44):24715-23.
31. Jumper J, Evans R, Pritzel A, Green T, Figurnov M, Ronneberger O, et al. Highly accurate protein structure prediction with AlphaFold. Nature. 2021;596(7873):583-9.
32. Fleming J, Magana P, Nair S, Tsenkov M, Bertoni D, Pidruchna I, et al. AlphaFold Protein Structure Database and 3D-Beacons: New Data and Capabilities. Journal of Molecular Biology. 2025;437(15):168967.
33. Mukai K, Kawata-Mukai M, Tanaka T. Stabilization of phosphorylated Bacillus subtilis DegU by DegR. J Bacteriol. 1992;174(24):7954-62.
34. Kobayashi K. Gradual activation of the response regulator DegU controls serial expression of genes for flagellum formation and biofilm formation in Bacillus subtilis. Molecular Microbiology. 2007;66(2):395-409.
35. Knudsen GM, Olsen JE, Dons L. Characterization of DegU, a response regulator in Listeria monocytogenes, involved in regulation of motility and contributes to virulence. FEMS Microbiology Letters. 2004;240(2):171-9.
36. Xi Y, Sohn AL, Joignant AN, Cologna SM, Prentice BM, Muddiman DC. SMART: A data reporting standard for mass spectrometry imaging. Journal of Mass Spectrometry. 2023;58(2):e4904.

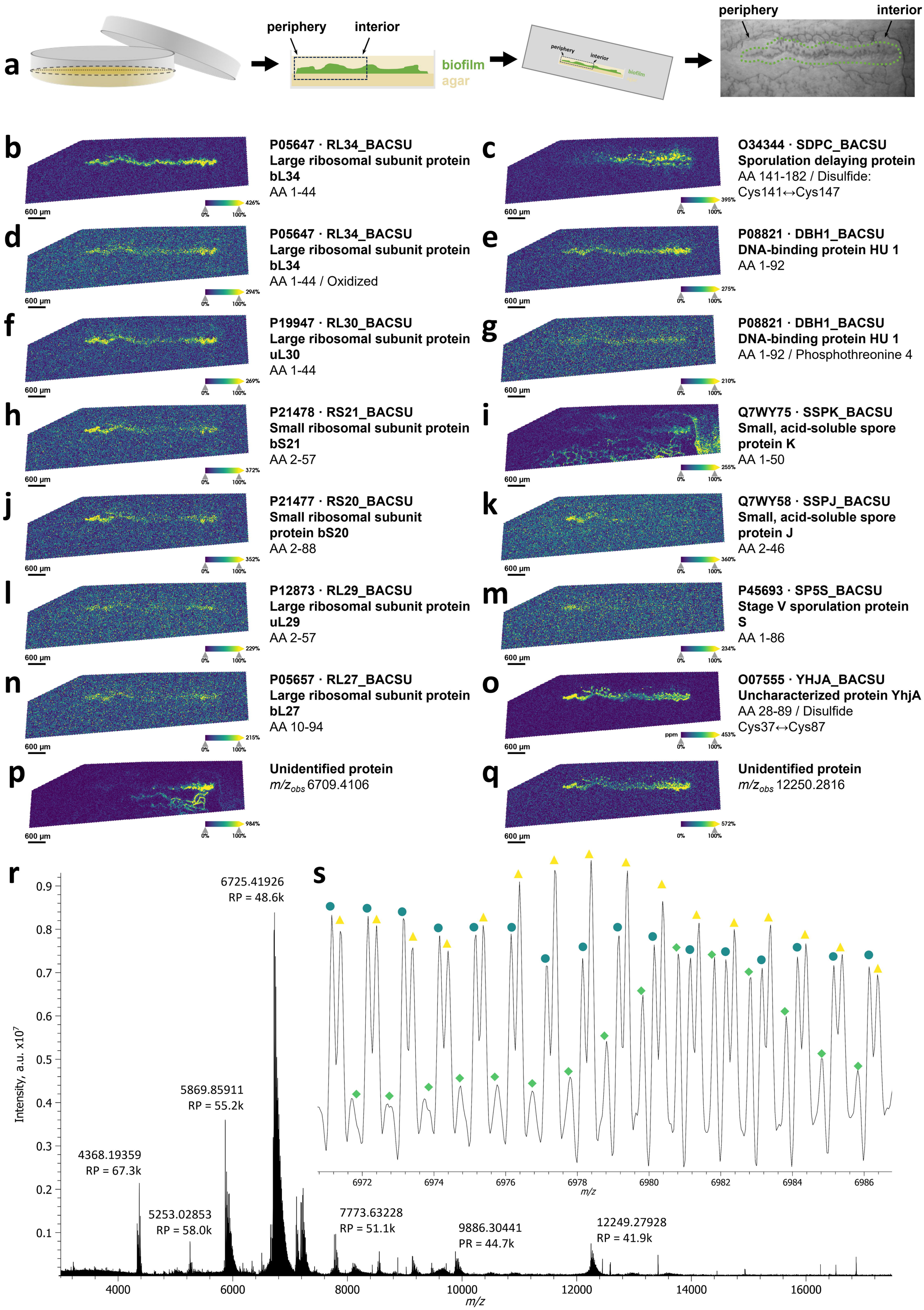
a
periphery
interior
biofilm
agar
b
P05647 · RL34_BACSU
Large ribosomal subunit protein bL34
AA 1-44
c
O34344 · SDPC_BACSU
Sporulation delaying protein
AA 141-182 / Disulfide: Cys141↔Cys147
d
P05647 · RL34_BACSU
Large ribosomal subunit protein bL34
AA 1-44 / Oxidized
e
P08821 · DBH1_BACSU
DNA-binding protein HU 1
AA 1-92
f
P19947 · RL30_BACSU
Large ribosomal subunit protein uL30
AA 1-44
g
P08821 · DBH1_BACSU
DNA-binding protein HU 1
AA 1-92 / Phosphothreonine 4
h
P21478 · RS21_BACSU
Small ribosomal subunit protein bS21
AA 2-57
i
Q7WY75 · SSPK_BACSU
Small, acid-soluble spore protein K
AA 1-50
j
P21477 · RS20_BACSU
Small ribosomal subunit protein bS20
AA 2-88
k
Q7WY58 · SSPJ_BACSU
Small, acid-soluble spore protein J
AA 2-46
l
P12873 · RL29_BACSU
Large ribosomal subunit protein uL29
AA 2-57
m
P45693 · SP5S_BACSU
Stage V sporulation protein S
AA 1-86
n
P05657 · RL27_BACSU
Large ribosomal subunit protein bL27
AA 10-94
o
O07555 · YHJA_BACSU
Uncharacterized protein YhjA
AA 28-89 / Disulfide Cys37↔Cys87
p
Unidentified protein
m/z_obs 6709.4106
q
Unidentified protein
m/z_obs 12250.2816
600 µm
0%
100%
r
s
Intensity, a.u. x10^7
m/z
6725.41926
RP = 48.6k
5869.85911
RP = 55.2k
4368.19359
RP = 67.3k
5253.02853
RP = 58.0k
7773.63228
RP = 51.1k
9886.30441
PR = 44.7k
12249.27928
RP = 41.9k

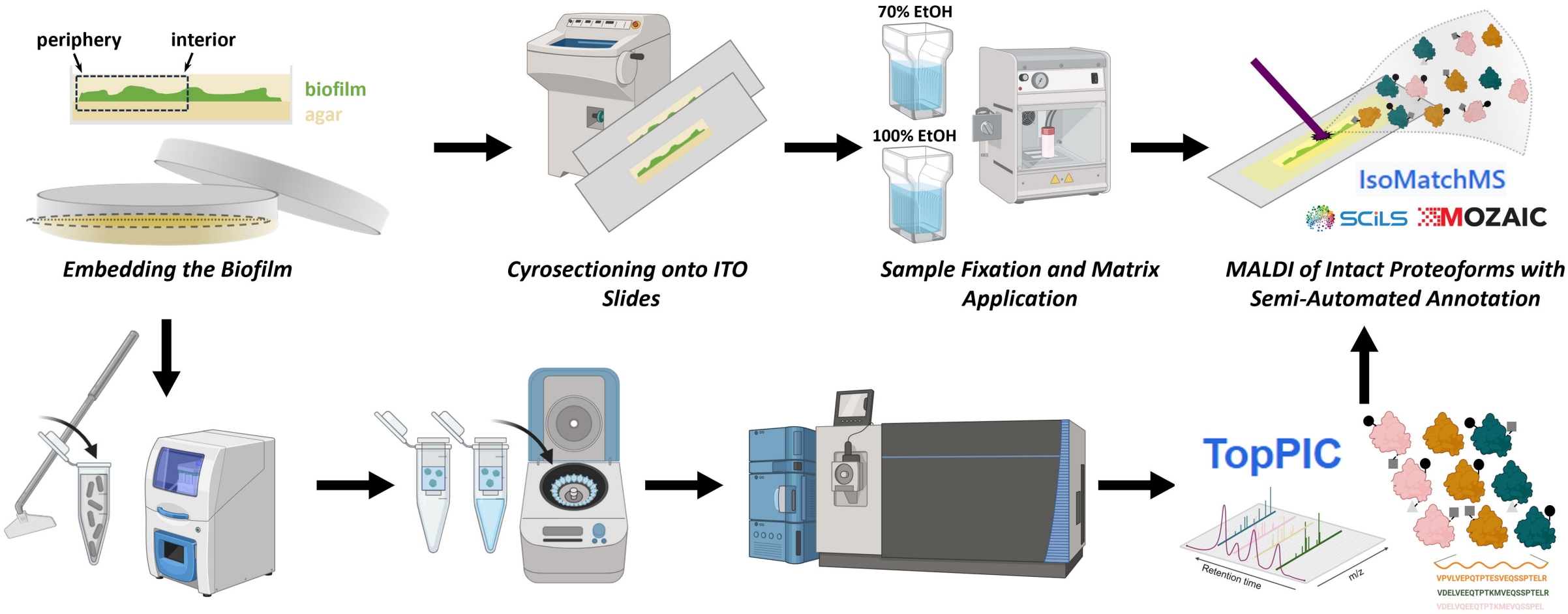
periphery
interior
biofilm
agar
Embedding the Biofilm
Cyrosectioning onto ITO Slides
70% EtOH
100% EtOH
Sample Fixation and Matrix Application
IsoMatchMS
SCiLS
MOZAIC
MALDI of Intact Proteoforms with Semi-Automated Annotation
Cell Scraping, Homogenization, and Extraction
Sample Resuspension, Filtration, and Concentration
Liquid Chromatography Mass Spectrometry of Intact Proteoforms
TopPIC
Retention time
m/z
VPVLVEPQTPTESVEQSSPTELR
VDELVEEQTPTKMVEQSSPTELR
VDELVQEEQTPTKMEVQSSPEL
Bioinformatics for Proteoform Database Generation